Quaternary Research (2021), **103**, 74–87
doi:10.1017/qua.2021.5

Research Article

Paleowind directions from the magnetic fabric of loess deposits in the western Chinese Loess Plateau and implications for dust provenance

Xinbo Gao[a], Qingzhen Hao[a,b,c], Junyi Ge[b,c,d], Long Han[e], Yu Fu[a,c], Xuechao Wu[a,c], Chenglong Deng[c,f], Slobodan B. Marković[g,h] and Zhengtang Guo[a,b,c]

[a]Key Laboratory of Cenozoic Geology and Environment, Institute of Geology and Geophysics, Chinese Academy of Sciences, No. 19 Beitucheng Western Road, Beijing, 100029, China; [b]CAS Center for Excellence in Life and Paleoenvironment, Beijing, 100044, China; [c]University of Chinese Academy of Sciences, No.19(A) Yuquan Road, Beijing, 100049, China; [d]Key Laboratory of Vertebrate Evolution and Human Origins of Chinese Academy of Sciences, Institute of Vertebrate Paleontology and Paleoanthropology, Chinese Academy of Sciences, P.O. Box 643, Beijing, 100044, China; [e]School of Environmental Science and Engineering, Southern University of Science and Technology, 1088 Xueyuan Road, Shenzhen, 518055, China; [f]State Key Laboratory of Lithospheric Evolution, Institute of Geology and Geophysics, Chinese Academy of Sciences, No. 19 Beitucheng Western Road, Beijing, 100029, China; [g]Faculty of Sciences, University of Novi Sad, Trg Dositeja Obradovića 3, Novi Sad, 21000, Serbia and [h]Serbian Academy of Sciences and Arts, Knez Mihajlova 35, Belgrade, 11000, Serbia

Abstract

The aeolian loess-paleosol sequences in the Chinese Loess Plateau (CLP) are an excellent archive of variations in atmospheric circulation in the geological past. However, there is no consensus regarding the roles of the East Asian winter monsoon and westerly winds in transporting the dust responsible for loess deposition during glacial and interstadial periods. We conducted detailed measurements of the anisotropy of magnetic susceptibility (AMS) on two parallel loess profiles covering the most recent 130 ka in the western CLP to determine paleowind directions. Results show that the magnetic lineations of the loess and paleosol units in both sections are significantly clustered along the northwest to southeast direction. These observations demonstrate that the prevailing wind system responsible for dust transport in the western CLP was the northwesterly winter monsoon, rather than the westerly winds. The AMS-derived dust-bearing wind direction was relatively stable during the last glacial and interglacial cycle in the western CLP, consistent with sedimentary and AMS evidence from the eastern CLP. Accordingly, it is reasonable to conclude that large areas of deserts and Gobi deserts areas located in the upwind direction were the dominant sources for the aeolian deposits of the Loess Plateau.

Keywords: Anisotropy of magnetic susceptibility (AMS), Loess, Paleowind direction, East Asian winter monsoon, Chinese Loess Plateau

(Received 28 August 2020; accepted 20 January 2021)

INTRODUCTION

Atmospheric circulation has long been recognized as an important mechanism for modulating regional and global climate via moisture and energy exchanges (Hadley, 1735; Manabe, 1969). In recent decades, there has been a growing awareness of the major influence of various components of atmospheric circulation (e.g., monsoons, jet streams, and storm tracks) on Earth systems via the transport of mineral dust (Arimoto, 2001; Ridgwell, 2002; Goudie and Middleton, 2006; Bullard, 2016). Atmospheric dust particles are an important agent of climate change via a variety of physical and biogeochemical mechanisms, including direct effects on Earth's radiative balance (Kinne and Pueschel, 2001; Sokolik et al., 2001), and iron fertilization effects that influence the oceanic carbon cycle and, in turn, atmospheric carbon dioxide concentration (Martin et al., 1994; Boyd et al., 2000). The extensive dryland areas in central Asia, occupied by the Gobi and other deserts (Fig. 1a), are an extremely active dust source. Modern meteorological data and model simulations suggest that long-range atmospheric dust transport from the Asian interior has important effects on the regional climate and even global circulation (Zhang et al., 2003; Guo et al., 2017). Accordingly, improving our knowledge of variations in atmospheric circulation in the Asian interior during the geological past is important for understanding global climate changes.

The loess-paleosol sequences of the Loess Plateau of north-central China potentially provide an excellent geological record of atmospheric circulation of the Asian interior, which functions as a link within the source-to-sink system of Asian dust deposition (Liu, 1985; Ding et al., 2002; Guo et al., 2002, 2008; Lu et al., 2010; Sun et al., 2012; Hao et al., 2012). Intensive geochronological studies of these sedimentary sequences, based mainly on magnetostratigraphy, have proposed an age of 22 Ma (Guo et al., 2002, 2008; Hao and Guo, 2007) for the initiation of the inland desert in Asia and the formation of a modern-like atmospheric circulation system (Guo et al., 2002, 2008).

Sedimentary evidence from loess deposits in the central Loess Plateau east of the Liupan Mountains suggests that the prevailing winds responsible for the dust transport are the northwesterly

Corresponding author: Qingzhen Hao, Email: haoqz@mail.iggcas.ac.cn

Cite this article: Gao X, Hao Q, Ge J, Han L, Fu Y, Wu X, Deng C, Marković SB, Guo Z (2021). Paleowind directions from the magnetic fabric of loess deposits in the western Chinese Loess Plateau and implications for dust provenance. *Quaternary Research* **103**, 74–87. https://doi.org/10.1017/qua.2021.5

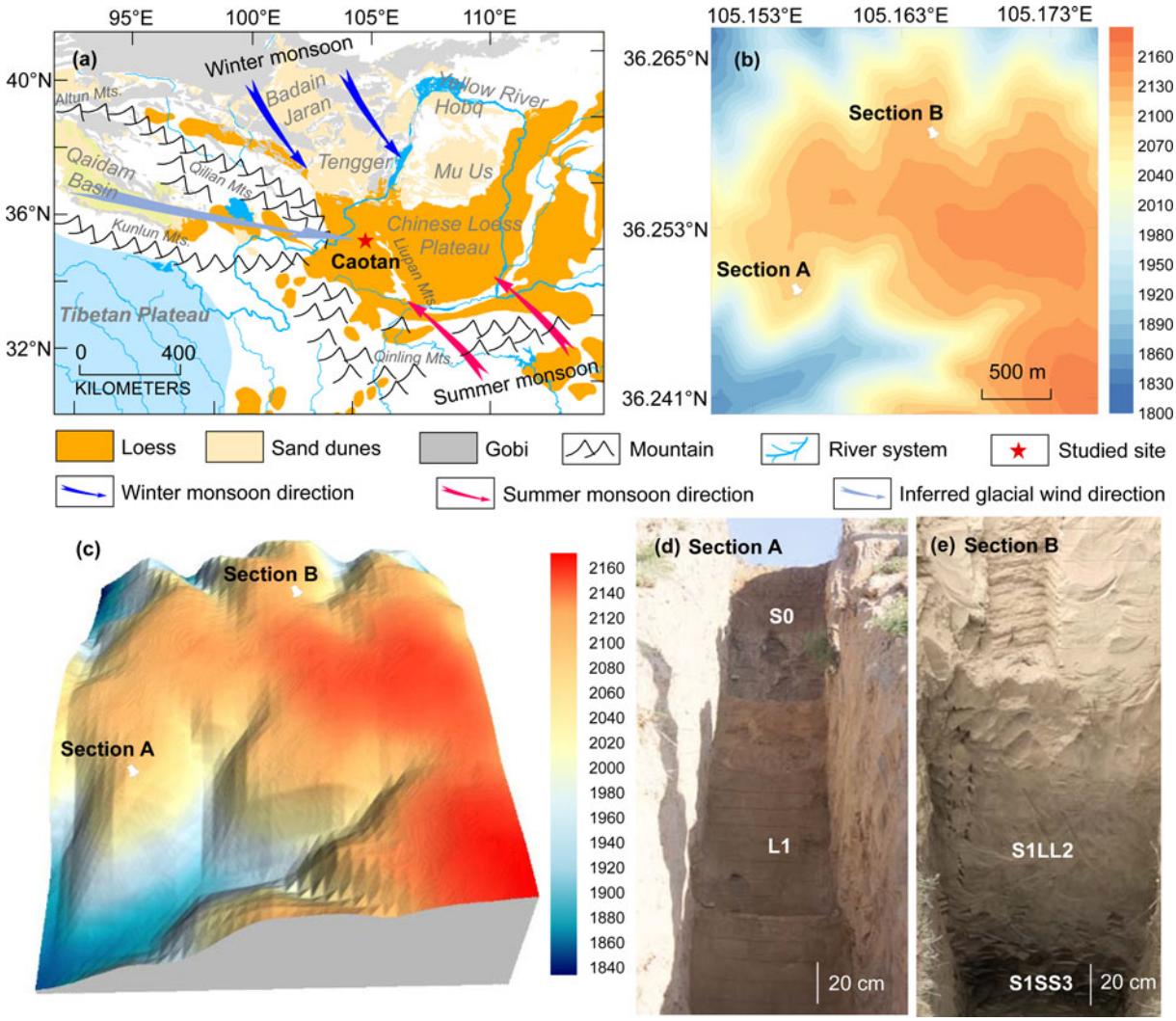

Figure 1. (color online) (a) Map showing study site in relation to the entire Chinese Loess Plateau, neighboring deserts, Gobi, basins, mountains, and river systems; arrows represent the approximate wind directions of the East Asian winter and summer monsoons and inferred glacial wind direction based on the provenance evidence of detrital zircon geochronology (Pullen et al., 2011). (b) Digital elevation model of Section A and Section B from the loess study site. Base map data downloaded at June 7, 2020 from https://maps.ngdc.noaa.gov/viewers/wcs-client. (c) Locations of loess sections A and B on a 3-D surface map with a same horizontal scale as (b). (d, e) Photographs of Section A and Section B. S0: the Holocene soil; L1: the last glacial loess; S1LL2: the second loess interlayer in the paleosol unit S1; S1SS3: the oldest soil interlayer in the paleosol unit S1.

winds of the East Asian winter monsoon. Based on detailed field surveys and laboratory measurements, Liu (1966) found a southeastward decrease in the grain size of loess deposits in the Eastern CLP, and accordingly, the thick loess deposits of the Loess Plateau were divided spatially from northwest to southeast into a sandy loess belt, a silty loess belt, and a clay loess belt. This pattern was verified by grain-size evidence from loess deposits spanning the past two glacial and interglacial cycles (Ding et al., 1999; Yang and Ding, 2008). Similar patterns have also been observed in the spatial variations of the thickness of the Quaternary loess sequences of the Loess Plateau, which decrease gradually from ~450 m in the northwestern Loess Plateau to 100–180 m in the central area (Liu, 1985; Lu and Sun, 2000). The spatial variations of the grain size and thickness of the loess deposits depend mainly on the direction and intensity of the dust-transporting winds (Pye and Tsoar, 1987). Therefore, the southeastward fining and thinning of the loess deposits suggests that the dust particles comprising the loess deposits in the main part of the CLP were transported by the northwesterly winter monsoon winds generated by the Siberian-Mongolian anticyclone (Wang, 2006).

However, some recent provenance evidence, based mainly on the U-Pb geochronology of single zircon grains, was used to propose that the westerly winds, rather than East Asian winter monsoon winds, dominated the dust transport responsible for loess deposition during glacials (Pullen et al., 2011). Comparison of zircon U-Pb age spectra of loess samples from the CLP and of sand samples from various source regions revealed that the loess samples from the Loess Plateau and sand samples from the Qaidam Basin share similar age distribution patterns. Thus, Pullen et al. (2011) proposed that the Qaidam Basin to the west of the CLP was the dominant source for dust contribution to the loess deposits, and that westerly winds have played a crucial role in transporting dust from western source areas towards the Loess Plateau during glacial and interstadial periods. In contrast, during interglacial periods, a different wind system, the northwest winds of the East Asia winter monsoon, were proposed as the dust-bearing winds (Pullen

https://doi.org/10.1017/qua.2021.5 Published online by Cambridge University Press

et al., 2011). Studies of wind erosion rates in the Qaidam Basin and the estimated volume of material removed by wind erosion also support the conclusion that the Qaidam Basin is a major source of dust to the CLP (Kapp et al., 2011; Rohrmann et al., 2013; Wu et al., 2019). Although Licht et al. (2016) ruled out the major dust contribution from the Qaidam Basin, they still stressed the influence of the westerly winds on dust transportation.

Using single geochemical tracers without considering related atmospheric circulation patterns may lead to misleading conclusions about dust provenance. The clastic materials of the Qaidam Basin originate mainly from the Kunlun and Qilian Mountains of the northeastern Tibetan Plateau (Wang et al., 2017; Nie et al., 2019; Fig. 1a). Recently, an increasing amount of geochemical evidence has shown that large-scale arid areas, which are major depositional areas of clastic materials of the northeastern Tibetan Plateau, have made a large contribution to the dust deposited in the CLP (Zhang et al., 2016; Li et al., 2018; Bird et al., 2020). Therefore, it is unsurprising that the zircon U-Pb age spectra of loess samples from the Loess Plateau and sand samples from the Qaidam Basin share some similar age peaks (Pullen et al., 2011); however, this does not mean that the Qaidam Basin was an important dust source for the CLP. Detailed reconstructions of paleowind directions can potentially resolve this issue. The western Loess Plateau (west of the Liupan Mountains) is closer to the Qaidam Basin than the rest of the plateau and is therefore well suited for evaluating the proposed role of westerly winds in transporting aeolian dust to the CLP. However, the limited area of loess distribution and complex topography of the western CLP hinder a systematic spatial analysis of sedimentary proxies such as grain size. As a result, there is a lack of paleowind evidence available from the western CLP.

The anisotropy of magnetic susceptibility (AMS), or magnetic fabric, is a useful approach for directly measuring paleowind directions from aeolian deposits. AMS is a physical property of sediments, reflecting differences in the magnetic susceptibility measured in different sample orientations, and it can be graphically expressed as a three-dimensional ellipsoid with maximum (κ_{max}), intermediate (κ_{int}), and minimum (κ_{min}) axes of susceptibility (Ising, 1943; Graham, 1954). AMS is dominantly controlled by the preferred crystallographic and dimensional orientations of anisotropic magnetic minerals within a sample (Owens and Bamford, 1976; Hrouda, 1982; Lowrie, 1989; Rochette et al., 1992). For windblown deposits such as loess, the preferred orientation of individual magnetic grains or grain clusters usually represents the prevailing direction of the dust-bearing winds. Therefore, the paleowind directions responsible for loess deposition can be determined directly by measuring the magnetic fabric. AMS measurements of loess samples from the CLP by Thistlewood and Sun (1991) revealed that the magnetic fabric of loess and paleosol samples was characterized by a WNW–ESE orientation of the κ_{max} axis, which suggested the East Asian winter monsoon winds were responsible for the dust transport. The relationship between the orientation of the κ_{max} axis of the magnetic fabric of aeolian deposits and wind direction was further verified by laboratory wind-tunnel experiments (Wu et al., 1998). Extensive AMS studies have subsequently been conducted on the loess deposits of the CLP of northern China (Zhu et al., 2004; Huang and Sun, 2005; Wang et al., 2007; Zhang et al., 2010; Liu and Sun, 2012; Ge et al., 2014; Peng et al., 2015), Europe (Nawrocki et al., 2006, 2018; Antoine et al., 2014; Taylor and Lagroix, 2015; Zeeden et al., 2015; Bradák et al., 2018), North America (Lagroix and Banerjee, 2002, 2004a, b), and Siberia (Matasova et al., 2001).

In the present study, detailed AMS analyses were conducted on two thick loess profiles from Caotan town, Huining county, in Gansu Province (Fig. 1). Both profiles span marine isotope stages 1–5 (i.e., the past 130 ka) according to the Chinese loess Chiloparts time scale of Ding et al. (2002). Our specific aims were to reconstruct the paleowind direction responsible for the loess deposits of the western CLP, and to investigate temporal variations of paleowind direction on glacial–interglacial timescales.

SETTING AND SAMPLING

The two loess profiles investigated herein, Section A and Section B (Fig. 1b–e), are located in Caotan town, northern Huining County, at an elevation of ~2,100 m asl, ~150 km from the southernmost part of the Tengger Desert, in the western part of the CLP (Fig. 1a). Under the influence of the East Asian monsoon, the summer season in the study area is characterized by warm and moist conditions with a prevailing southeasterly wind (summer monsoon), while the winter season is characterized by cold and dry conditions with a prevailing northerly or northwesterly wind (winter monsoon). The mean annual precipitation and temperature at Huining are ~359 mm and ~7.7°C, respectively. The distance from Section A to Section B is ~1.5 km. Two parallel profiles were studied in order to ensure reliability of the results. Field observation revealed that both sections consist of an uppermost dark loamy soil (S0), a thick, yellow-orange loess layer (L1), and a pedocomplex (S1) (Fig. 1d); S1 can be subdivided into five layers: two less developed bright-brown soils in the upper part (S1SS1 and S1SS2), and one better developed dark-brown soil (S1SS3) in the lower part (Fig. 1e), interbedded with two orange loess beds (S1LL1 and S1LL2). The thicknesses of Section A and Section B are ~21.0 m and 24.3 m, respectively.

Block samples with dimensions $10 \times 10 \times 10$ cm^3 and oriented with a magnetic compass were collected from both sections. The sampling intervals for Section A were 5–10 cm for the upper 15 m (S0 and L1) and 2.5 cm for the lower 6 m (S1), and 415 oriented samples were collected. For Section B, 484 oriented samples were collected at a sampling interval of 5 cm. In the laboratory, cubic samples of 8 cm^3 volume were cut from the block samples for AMS and magnetic susceptibility measurements.

METHODS

To identify the magnetic mineral assemblages of the studied loess deposits, temperature-dependent magnetic properties and hysteresis properties were measured on representative loess and paleosol samples collected from Section A and Section B. The high-temperature dependence of magnetic susceptibility was measured with an MFK1-FA multi-function Kappabridge with a CS4 high-temperature control unit. Approximately 0.3 g of powdered sample was heated from room temperature to 700°C, then cooled down to room temperature in an argon atmosphere. The magnetic susceptibility was measured in a field intensity of 200 Am^{-1} and a frequency of 976 Hz. Low-temperature thermal demagnetization of saturation isothermal remanent magnetization (LT-SIRM) measurements were conducted on a Quantum Designs Magnetic Properties Measurement System. After cooling to 15 K in zero field, SIRM was imparted in a field of 2.5 T. The sample was then warmed up to 300 K at a constant rate of 3 K/min, and the variation in remanence was measured repeatedly in a field-free space. First-Order Reversal Curve (FORC) measurements were performed on a MicroMag 3900 vibrating sample magnetometer (VSM 3900). 100 FORCs were measured with a

https://doi.org/10.1017/qua.2021.5 Published online by Cambridge University Press

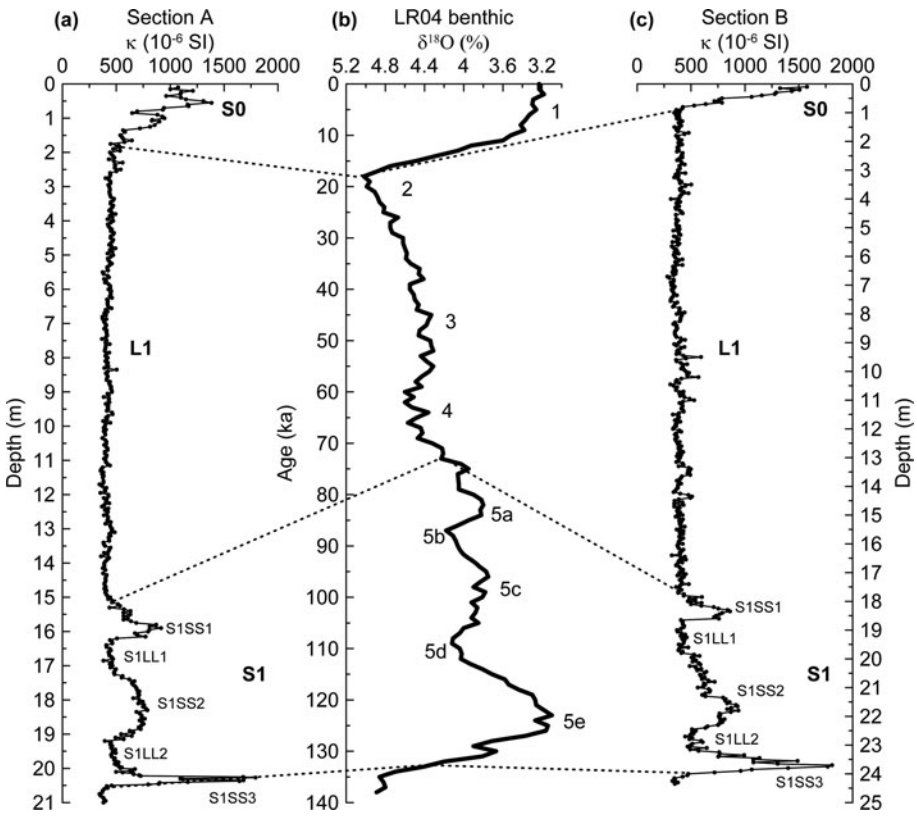

Figure 2. Variation of the volume-specific magnetic susceptibility (κ) as a function of depth for loess sections A and B and its correlation with the LR04 benthic $\delta^{18}O$ stack marine isotope stages (MIS) of Lisiecki and Raymo (2005). S0: the Holocene soil; L1: the last glacial loess; S1: the last interglacial soil; S1SS1, S1SS2, and S1SS3: the youngest, second, oldest subsoil interlayers in the paleosol unit S1, respectively; S1LL1, and S1LL2: the first, and second loess interlayer in the paleosol unit S1, respectively.

maximum field of 1.0 T. The FORC data were processed using FORCinel software (Harrison and Feinberg, 2008).

The AMS of each oriented specimen was measured using an MFK1-FA multi-function Kappabridge instrument (Agico Ltd., Brno) with an automated sample handling system, at an operating frequency of 976 Hz and field intensity of 200 Am^{-1}. Each sample was rotated through three orthogonal planes. The resulting AMS ellipsoid was calculated using the least-squares method, following Jelinek (1981). The anisotropy parameters used here are foliation (F), lineation (L), and the degree of anisotropy (P), and were calculated using Anisoft software based on the statistical methods of Jelinek (1981) and Constable and Tauxe (1990). The relevant calculations are: Foliation $(F) = \kappa_{int}/\kappa_{min}$; Lineation $(L) = \kappa_{max}/\kappa_{int}$; Degree of anisotropy $(P) = \kappa_{max}/\kappa_{min}$.

RESULTS

Magnetic susceptibility (κ)

Depth profiles of the volume magnetic susceptibility of Section A, Section B, and their correlations with the marine oxygen-isotope record (Lisiecki and Raymo, 2005) are illustrated in Figure 2. Previous studies of the loess deposits in the western CLP have established a robust scheme of correlations between loess units and the sequence of marine isotope stages (MIS) (Ding et al., 2002; Sun and Huang, 2006). As expected, the soil layers are characterized by higher κ values and loess layers by lower values (Fig. 2a, c). The κ records for the two sections can be correlated peak by peak; four prominent peaks corresponding to S0, S1SS1, S1SS2, and S1SS3 can be readily correlated with warmer intervals MIS 1, MIS 5a, MIS 5c, and MIS 5e of the marine oxygen isotope record (Fig. 2). Both field observations and the κ records indicate that the strongly developed soil layer S1SS3 formed during MIS 5e.

Magnetic mineralogy

The heating curves of the high-temperature dependence of magnetic susceptibility (χ) are shown in Figure 3. Overall, the loess and paleosol samples showed a similar pattern: below ~280°C there was a steady rise in the χ, which is likely due to the gradual unblocking of fine-grained single domain (SD) particles (Deng et al., 2000; Liu et al., 2005), and from ~280°C to ~440°C, the reduction in χ primarily originated from the conversion of metastable maghemite to hematite (Deng et al., 2000, 2005; Zhao et al., 2017; Gao et al., 2019). The susceptibility loss is more prominent in the paleosol samples than in the loess samples, suggesting a higher content of fine-grained pedogenic maghemite particles in the former. Notably, the susceptibility hump at ~510°C is commonly attributed to the neoformation of magnetite from iron-bearing silicates during heating (Deng et al., 2000; Liu et al., 2005), which is confirmed by the significantly enhanced susceptibility after cooling to room temperature in the cooling curves (not shown). At ~585°C, the sharp decrease in χ corresponds to the Curie point of nearly stoichiometric magnetite.

LT-SIRM warming curves for the selected loess and paleosol samples are shown in Figure 4. An abrupt drop in the intensity of remanence at ~120 K is evident in the loess samples (Fig. 4a, b), consistent with the normalized first-order derivative of LT-SIRM curves (Fig. 4c, d), which indicates the Verwey transition of the nearly stoichiometric magnetite (Rochette et al., 1990; Özdemir et al., 1993). The paleosol samples show a much less marked Verwey transition at ~120 K, as in this case, the detrital coarse magnetic grains are usually masked by fine-grained pedogenic ferrimagnets and the low-temperature oxidation of coarse-grained magnetite (Banerjee et al., 1993).

The FORC diagrams of the loess and paleosol samples are shown in Figure 5. The divergent outer contours for the loess

https://doi.org/10.1017/qua.2021.5 Published online by Cambridge University Press

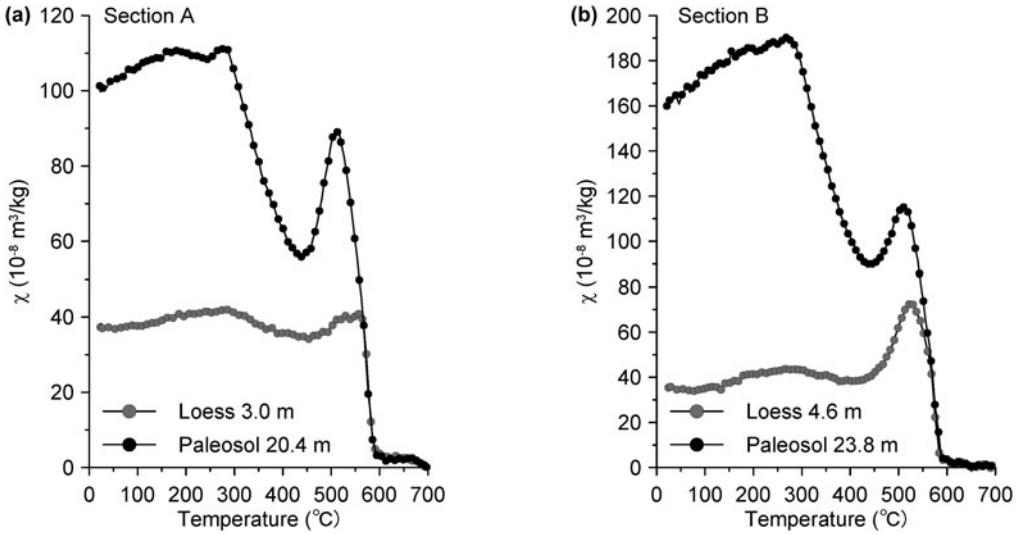

Figure 3. Heating curves of the temperature-dependence of magnetic susceptibility of representative loess and paleosol samples.

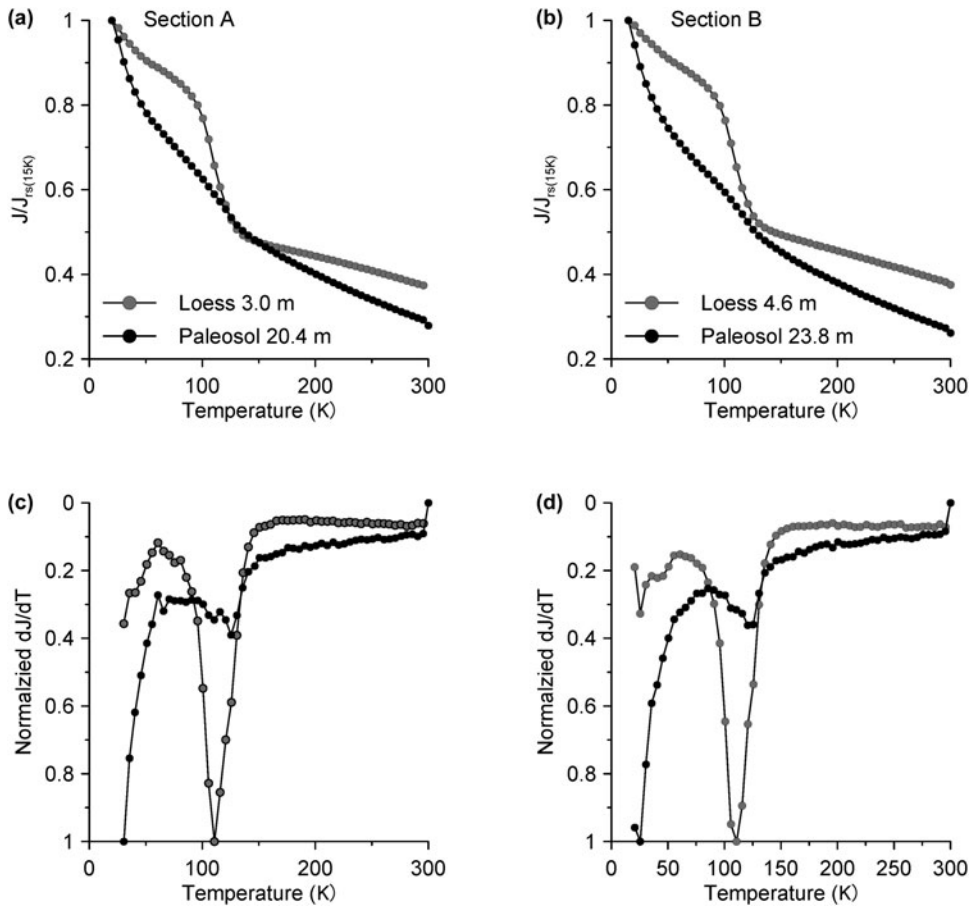

Figure 4. Low-temperature thermal demagnetization of saturation isothermal remanent magnetization (LT-SIRM) acquired in 2.5 T at 15 K (a, b) and normalized first-order derivative of LT-SIRM curves (c, d) for representative loess and paleosol samples.

samples indicate the presence of coarse-grained pseudo-single domain (PSD) or multidomain (MD) particles (Muxworthy and Dunlop, 2002; Smirnov, 2006; Roberts et al., 2014), consistent with the low-temperature magnetic properties (Fig. 4). In contrast, the paleosol samples are characterized by tightly closed inner contours with negligible vertical spread, indicating the presence of magnetically non-interacting SD particles. Additionally, the observed secondary peaks at the origin of the FORC diagram indicate the presence of superparamagnetic (SP) particles (Pike et al., 2001; Roberts et al., 2000). Fine-grained SP and SD particles

https://doi.org/10.1017/qua.2021.5 Published online by Cambridge University Press

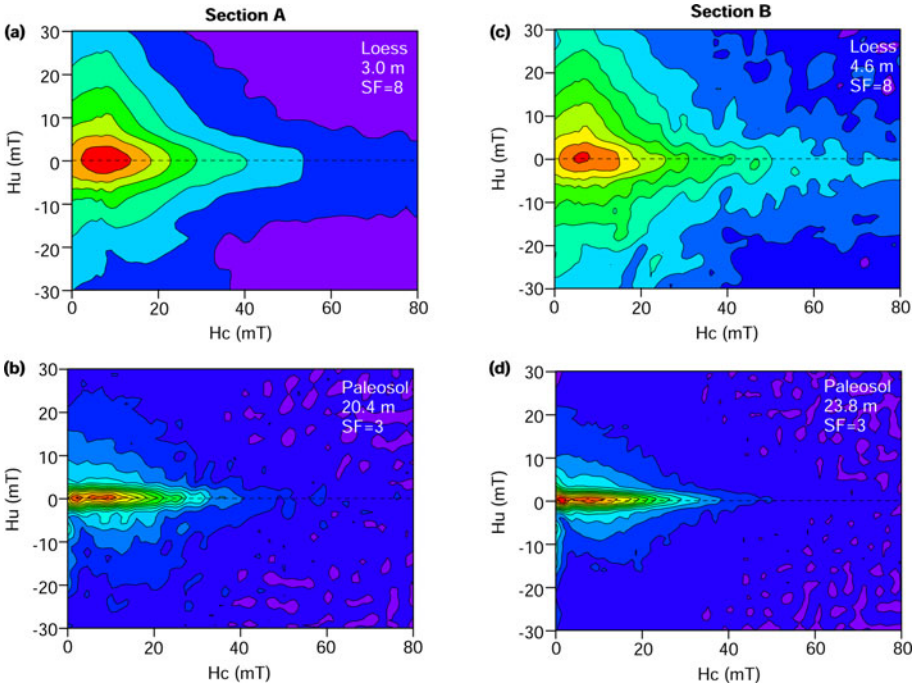

Figure 5. (color online) First-Order Reversal Curve (FORC) diagrams for representative loess and paleosol samples collected from Section A (a, b) and Section B (c, d). Loess samples show divergent outer contours, indicating coarse-grained pseudo-single domain (PSD) or multidomain (MD) particles (Muxworthy and Dunlop, 2002; Smirnov, 2006; Roberts et al., 2014). Paleosol samples show tightly closed inner contours with negligible vertical spread, indicating the presence of magnetically non-interacting SD particles. Secondary peaks at the origin indicate presence of superparamagnetic (SP) particles (Pike et al., 2001; Roberts et al., 2000). SF: smoothing factor; higher SFs were used for the loess samples to enhance the signal to noise ratio.

in paleosol layers have been demonstrated to originate mainly from neo-formed maghemite during pedogenesis (Zhou et al., 1990; Maher and Thompson, 1991; Verosub et al., 1993), which is in accordance with our thermomagnetic results (Fig. 3). This suggests a higher maghemite content in the paleosol samples.

In summary, our rock magnetic investigations revealed that magnetic assemblages of loess samples mainly consist of detrital coarse-grained PSD or MD magnetite. For paleosol samples, both the pedogenic fine-grained SP and SD maghemite and the detrital coarse-grained PSD or MD magnetite dominate the magnetic assemblages.

Anisotropy of magnetic susceptibility (AMS)

The anisotropy parameters ε_{12} and F_{12} have been widely used to evaluate the statistical significance of AMS data (Zhu et al., 2004; Lagroix and Banerjee, 2004b), where the notations 1 and 2 of these parameters are assigned to the maximum susceptibility axis (κ_{max}) and the intermediate susceptibility axis (κ_{int}), respectively. At the specimen level, ε_{12} is defined as the half-angular uncertainty of κ_{max} within the magnetic foliation plane, and represents the 95% confidence uncertainty ellipse of κ_{max}. The maximum allowable statistically significant ε_{12} is 22.5°, yielding a confidence ratio of 1.0 (Lagroix and Banerjee, 2004b). In addition, anisotropy data with $F_{12} > 4$ are statistically significant (Zhu et al., 2004). The AMS data (Fig. 6a, b) show that the results are statistically significant. Specimens with $\varepsilon_{12} < 22.5°$ and $F_{12} > 4$ account for 80.2% and 50.6% of the total data in Section A and Section B, respectively.

In general, Section A and Section B have comparable AMS characteristics. Inverse relationships between ε_{12} and the magnetic lineation (L) are evident (Fig. 6c, d), which can be attributed to the increase in random measurement errors for κ_{max} in the lineation plane with weak lineation. Both sections show stronger positive correlations between the degree of anisotropy P and magnetic foliation F (Fig. 6e, f), which suggests that the anisotropy is mainly controlled by the magnetic foliation. Data for almost all of the specimens are close to the foliation axes, consistent with previous studies of the AMS of loess deposits, indicating an oblate AMS ellipsoid for the specimens (Fig. 6g, h).

Stereographic projections of all specimens from Section A and Section B are plotted in Figures 7 and 8, respectively. The orientation of κ_{max} and κ_{min} are described by the declination (Dec-κ_{max} and Dec-κ_{min}), and the inclination (Inc-κ_{max} and Inc-κ_{min}). For Section A and Section B, specimens with Inc-$\kappa_{min} > 70°$ account for 72.0% and 72.9% of the total number of specimens, respectively, indicating a primary aeolian magnetic fabric without significant post- depositional disturbance (Figs. 7, 8).

To better understand possible variations in paleowind variations between glacial and interglacial cycles, each section was divided into three units: Holocene soil (S0), last glacial loess (L1), and last interglacial soil (S1). To improve the statistical significance of the principal orientations, specimens with $\varepsilon_{12} > 22.5°$ and Inc-$\kappa_{min} < 70°$ were removed, following Lagroix and Banerjee (2004b). Along with the stereographic projections, contour lines and rose diagrams are used to illustrate the distribution of κ_{max}. For each unit, the changes in orientation distributions between the initial dataset (Figs. 7a, 8a) and the selected dataset with $\varepsilon_{12} > 22.5°$ and Inc-$\kappa_{min} < 70°$ removed are shown (Figs. 7b, 8b).

For Section A, the stereographic projections for all specimens show that the κ_{max} is distributed along the NW–SE direction, and that κ_{min} forms a tight cluster around the vertical (Fig. 7a). The NW–SE directions of the κ_{max} declinations are more evident in the contour and rose diagrams (Figs. 7a, b). The stereographic projections of the selected specimens with $\varepsilon_{12} < 22.5°$ and Inc-$\kappa_{min} > 70°$ show similar characteristics (Fig. 7b). Unit S0 has a random distribution of κ_{max} and κ_{min} axes. For unit L1, the κ_{max} declination is mainly distributed in the NW, NE, and SE regions, the majority of the κ_{max} values are oriented along the NE–SW direction (Dec-$\kappa_{max} = 328.6°$), and κ_{min} values are clustered around the vertical (Fig. 7b; Table 1). The specimens from paleosol S1 also show a preferential alignment of κ_{max}

https://doi.org/10.1017/qua.2021.5 Published online by Cambridge University Press

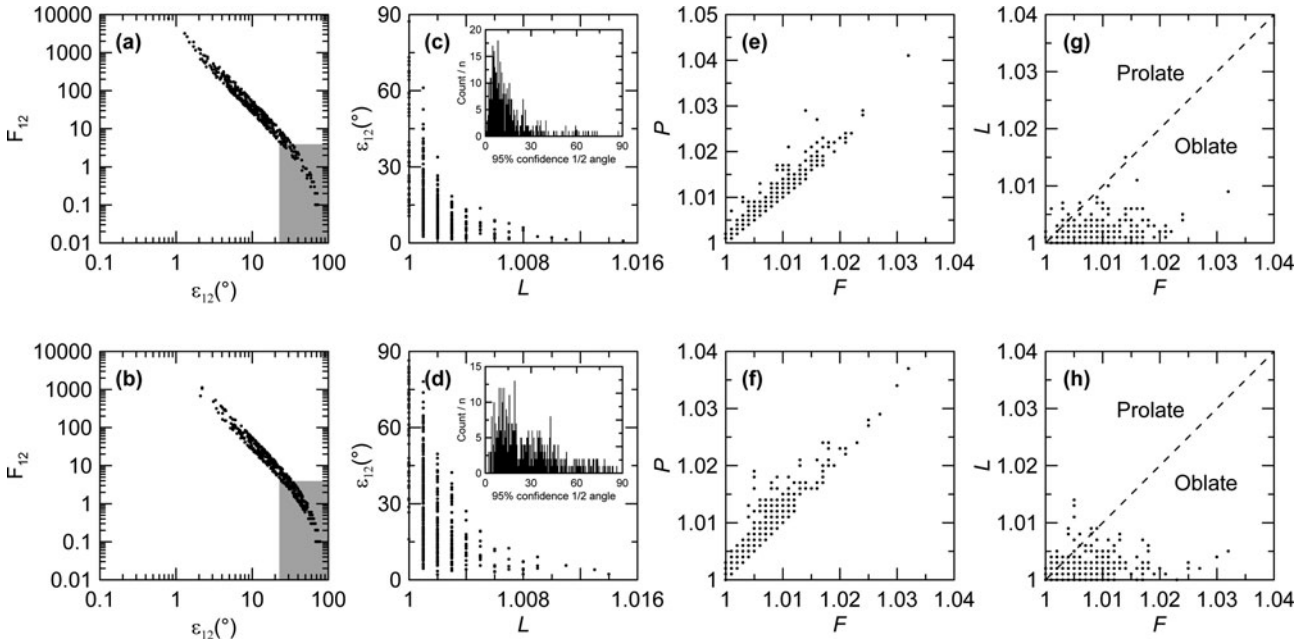

Figure 6. Statistical significance, angular uncertainties, and relationships between the anisotropy of magnetic susceptibility (AMS) parameters of the loess profiles of Section A (top; a, c, e, g) and Section B (bottom; b, d, f, h). The AMS data in (a, b) show results are statistically significant. Gray shading indicates plots with $\varepsilon_{12} >$ 22.5° and F12 < 4. Insets in (c, d) are frequency distributions of ε_{12} using a 1° bin size. Both sections show stronger positive correlations between the degree of anisotropy *P* and magnetic foliation *F* (e, f). Data for most samples are close to the foliation axes, indicating an oblate AMS ellipsoid (g, h). Magnetic lineation: *L*.

along NW–SE direction (Dec-κ_{max} = 150.6°) (Fig. 7b; Table 1). The κ_{min} inclinations are tightly vertical without significant deviation.

For Section B, the stereographic projections for all specimens show that the majority of κ_{max} directions are oriented along the NNW–SSE direction, and the κ_{min} inclinations are scattered around the vertical axis (Fig. 8). The specimens from paleosol S0 have highly scattered κ_{max} declinations and κ_{min} inclinations, which are not suited for further analysis. For unit L1, the κ_{max} directions are distributed along a girdle, oriented towards the NW–EW direction (Dec-κ_{max} = 347.5°). The preferred orientations of κ_{max} for the loess units from Section A and Section B are close to each other (Dec-κ_{max} = 328.6° for Section A; Dec-κ_{max} = 347.5° for Section B). The κ_{max} directions of paleosol S1 are also biased towards NW–SE (Dec-κ_{max} = 319.8°).

DISCUSSION

Evidence from theoretical calculations, laboratory wind-tunnel experiments, and the analysis of sedimentary deposits demonstrate that the primary aeolian fabric of loess deposits is an effective tool for determining the prevailing directions of the dust-bearing winds (Hrouda, 1982; Rochette et al., 1992; Wu et al., 1998; Lagroix and Banerjee, 2002). Although extensive AMS studies have been carried out on the loess deposits of the CLP during the past two decades, no consensus exists regarding the wind system responsible for the formation of the magnetic fabric of the loess deposits.

Three wind systems have been proposed to be responsible for the formation of the magnetic fabric of the loess deposits of the CLP: the northwesterly winter monsoon, the southeasterly summer monsoon, and the near-surface winds of the East Asian winter monsoon. The AMS study of Thistlewood and Sun (1991) revealed a NW–SE orientation of the κ_{max} axes, which is roughly parallel to the direction of the East Asian winter monsoon. Accordingly, the northwesterly winter monsoon was suggested to be the prevailing wind responsible for the formation of the magnetic fabric of the loess deposits. Zhang et al. (2010) found that the Inc-κ_{min} values of the AMS of three loess sections in the CLP (Baicaoyuan, Xifeng, and Yichuan) were all oriented towards the NW. They proposed that during rainy periods, the East Asian summer monsoon would result in the rearrangement and fixation of magnetic particles, and as a result, the summer monsoon was responsible for the formation of the magnetic fabric of the loess deposits. Zhu et al. (2004) observed that the dominant directions of Dec-κ_{max} of the AMS of the Lingtai loess section were oriented towards the NE during glacial periods, and toward the NW during interglacial periods. Considering the geographical location of the Lingtai section, close to the Liupan Mountains, Zhu et al. (2004) speculated that the direction of the winter monsoon of the study area might be influenced by the surrounding mountains. Ge et al. (2014) conducted detailed AMS studies of 10 loess sections of the last glacial period in the CLP, and their results showed that directions of Dec-κ_{max} were roughly consistent with the directions of the regional surface wind flow, including not only the northwesterly wind related to the large-scale east Asian winter monsoon but also with local winds, which are strongly influenced by regional topography, and concluded both winds are responsible for the formation of the magnetic fabric of the loess deposits.

With these previous studies in mind, it is reasonable to conclude that the magnetic fabric of the loess deposits used in our study, especially the loess units, is mainly generated by large-scale atmospheric circulation. The Caotan site is located in the northwestern CLP (Fig. 1a), near the modern northern limit of the East Asian summer monsoon, and loess deposits in this region have experienced a relatively low degree of pedogenesis compared with other regions of the CLP. Our field investigations showed

https://doi.org/10.1017/qua.2021.5 Published online by Cambridge University Press

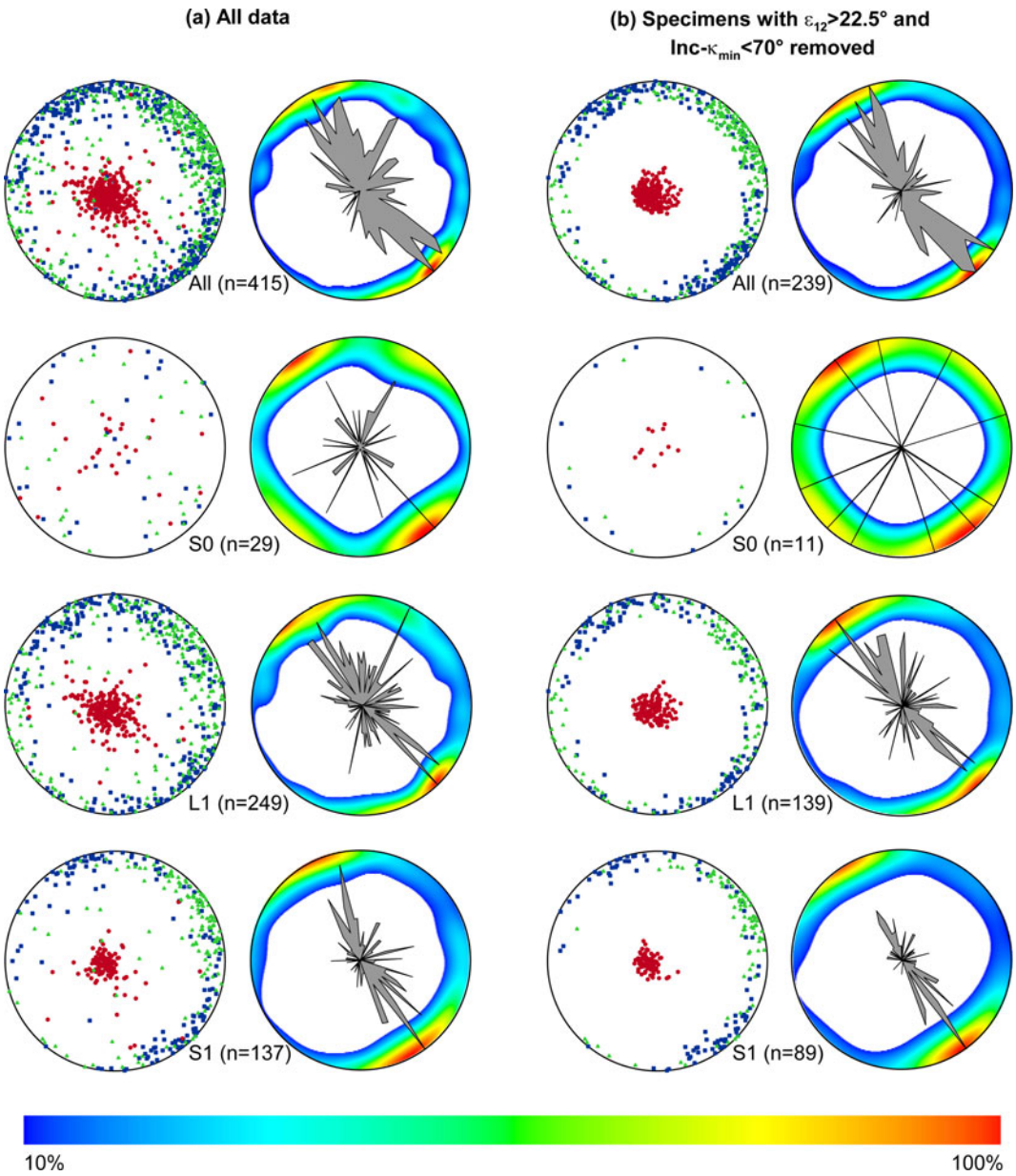

Figure 7. Lower hemisphere equal-area stereographic projections of AMS data from loess and paleosol units of Section A. (a) AMS results for all specimens. (b) AMS results with $\varepsilon_{12} > 22.5°$ and Inc-$\kappa_{min} < 70°$ excluded. S0: the Holocene soil; L1: the last glacial loess; S1: the last interglacial soil. For each dataset, the stereonet on the left shows the AMS data for the principal susceptibility axes, κ_{max} (blue squares), κ_{int} (green triangles), and κ_{min} (red dots). The stereonet on the right shows contours and rose diagrams for for the AMS data for the principal susceptibility axis, κ_{max}. (For interpretation of the references to color in this figure legend, the reader is referred to the web version of this article.)

that the loess layers in the area are characterized by a loose structure, light color, and coarse grain size, which indicates a low degree of pedogenic alteration. This conclusion was verified by our rock magnetic analyses, which revealed that the magnetic assemblage of the loess units mainly consists of coarse-grained PSD or MD particles (Figs. 4, 5). The weak pedogenic development of the loess layers indicates the limited influence of monsoon rainfall on the formation of the magnetic fabric. Our study area is also located in the northernmost part of the Liupan Mountains, and the limited elevation and size of the adjacent mountains do not significantly affect the direction of the large-scale atmospheric circulation. Finally, the loess landforms in Caotan town are mainly 'Yuan-type,' which are characterized by an extensive flat surface (Fig. 1). The loess deposits in Yuan-type landforms with horizontal bedding are usually conducive to settlement and preservation of dust particles, and, in turn, to the formation of a magnetic fabric without significant disturbance. Therefore, it is reasonable to conclude that the magnetic fabric of the loess deposits of the Caotan sections is mainly produced by large-scale atmospheric circulation, which is responsible for the dust transport.

Due to pedogenic processes, the environmental interpretation of the AMS for the paleosol layers alternating within the loess layers seems more complex. It has been suggested that enhanced weathering and maghemitization decreases the anisotropy degree, and also scatters anisotropy directions (Mathé et al., 1997). In the

https://doi.org/10.1017/qua.2021.5 Published online by Cambridge University Press

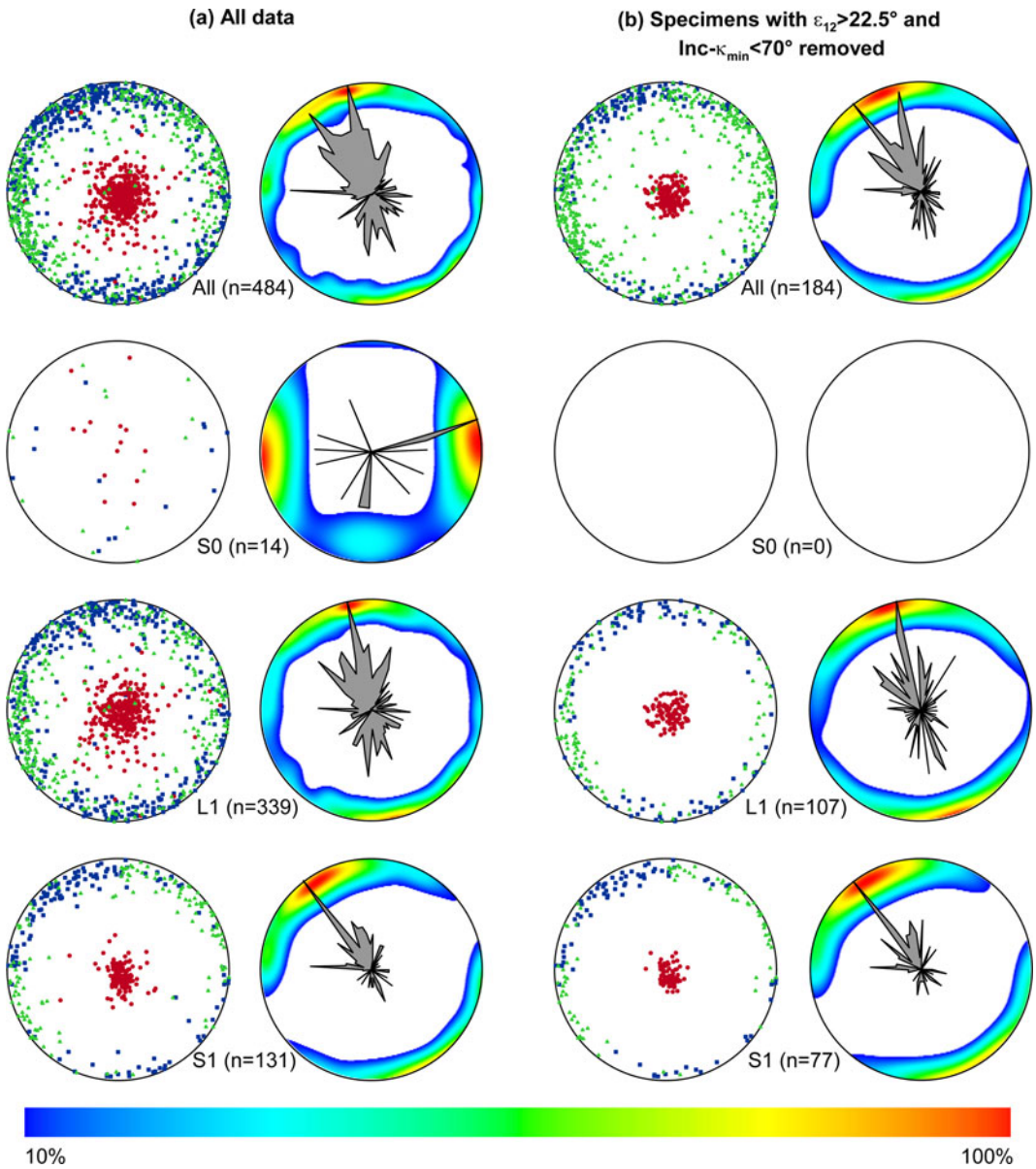

Figure 8. Lower hemisphere equal-area stereographic projections of AMS data from loess and paleosol units of Section B. (a) AMS results for all specimens. (b) AMS results with $\varepsilon_{12} > 22.5°$ and Inc-$\kappa_{min} < 70°$ removed. S0: the Holocene soil; L1: the last glacial loess; S1: the last interglacial soil. For each dataset, the stereonet on the left shows the AMS data for the principal susceptibility axes, κ_{max} (blue squares), κ_{int} (green triangles), and κ_{min} (red dots). The stereonet on the right shows contours and rose diagrams for the AMS data for the principal susceptibility axis, κ_{max}. (For interpretation of the references to color in this figure legend, the reader is referred to the web version of this article.)

studied area, our field observations found that the paleosol layers in sections A and B are mostly characterized by having a bright- to dark-brown color with granular structure, indicating relatively stronger pedogenesis during interglacials with enhanced monsoon rainfall and ambient temperature (Liu, 1985). Our rock magnetic results also indicate an increased concentration of pedogenic fine-grained (SP+SD) maghemite in paleosol samples (Figs. 3, 5). There is also a relatively lower degree of anisotropy (P) in the paleosol layers (S0 and S1) as compared to that of the coupled loess layers (Fig. 9), possibly indicating disturbance from the pedogenic processes. These observations indicate that magnetic fabrics of paleosol layers were possibly influenced by the process of soil formation. However, no significant difference was observed in the mean orientations of AMS axes between the last glacial loess (L1) and the last interglacial soil (S1) in both sections (Figs. 7, 8), possibly suggesting inheritance of the primary depositional fabric of the paleosol layers. The noticeable Verwey transition of the paleosol samples (Fig. 4) also robustly demonstrates the presence of primary coarse-grained magnetite. Given these observations, paleosols of the study area likely have a composite fabric of depositional and pedogenic fabrics. The scattered anisotropy directions of the Holocene soil (S0) in both sections possibly resulted from a lower degree of consolidation and disturbance from ancient human activities. Other studies proposed that the primary aeolian magnetic fabric of loess deposits could also be influenced by post-depositional processes (Hrouda, 1982; Ellwood, 1984; Tarling and Hrouda, 1993; Hus, 2003), such as compaction, freeze-thaw cycles, post-depositional deformation

https://doi.org/10.1017/qua.2021.5 Published online by Cambridge University Press

Table 1. Principal AMS orientation analysis. (a) Samples with $\varepsilon_{12} > 22.5°$ and Inc-$\kappa_{min} < 70°$ included; (b) Samples with $\varepsilon_{12} > 22.5°$ and Inc-$\kappa_{min} < 70°$ removed. S0: the Holocene soil; L1: the last glacial loess; S1: the last interglacial soil. Abbreviations: n = sample number; Dec. = declination; Inc = inclination; Max. = maximum angles of the 95% confidence ellipse; Min = minimum angles of the 95% confidence ellipse.

		Mean maximum eigenvector				Mean intermediate eigenvector				Mean minimum eigenvector			
				95% conf. ellipse				95% conf. ellipse				95% conf. ellipse	
Horizon	n	Dec.	Inc.	Max.	Min.	Dec.	Inc.	Max.	Min.	Dec.	Inc.	Max.	Min.
(a)													
Section A													
S0	29	19.8	3.3	81.7	27.0	109.9	2.5	81.7	23.0	237.3	85.9	31.3	22.0
L1	249	339.6	2.4	63.8	12.8	70.0	8.3	63.8	12.5	233.9	81.3	14.4	10.8
S1	137	148.1	1.7	75.4	8.3	57.9	7.6	75.4	6.6	250.9	82.2	8.7	6.4
Section B													
S0	14	87.6	3.2	26.2	15.0	178.0	7.5	26.5	21.7	334.7	81.8	22.3	15.5
L1	339	338.3	1.4	62.0	11.1	248.2	2.8	62.0	14.0	94.5	86.9	14.4	10.5
S1	131	323.2	7.4	55.5	7.9	53.4	1.3	55.5	7.0	153.3	82.5	8.3	6.8
(b)													
Section A													
S0	11	172.9	3.6	61.3	9.5	82.7	3.6	61.3	11.8	307.7	84.9	14.4	9.3
L1	139	328.6	1.2	45.2	8.7	58.7	6.0	45.2	8.6	227.0	83.9	9.1	8.4
S1	89	150.6	2.3	37.2	6.3	60.4	6.9	37.2	5.1	258.9	82.8	6.3	5.2
Section B													
S0	0												
L1	107	347.5	0.8	48.0	8.7	257.5	3.7	48.0	9.3	89.6	86.3	9.7	8.4
S1	77	319.8	6.9	53.1	6.4	50.0	1.6	53.1	5.1	152.8	82.9	6.8	5.0

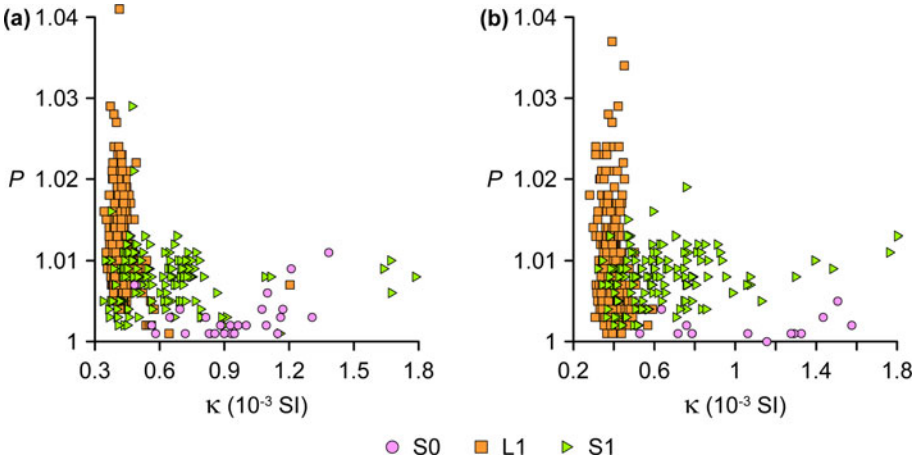

Figure 9. (color online) Plot of magnetic susceptibility (κ) versus degree of anisotropy (*P*) for loess deposits in (a) Section A and (b) Section B. A lower degree of anisotropy in paleosol layers S0-the Holocene soil and S1-the last interglacial soil than that in the coupled loess layers (L1-the last glacial loess) may indicate a disturbance from the pedogenic processes, and that magnetic fabrics of paleosol layers may have been influenced by the process of soil formation.

(Lagroix and Banerjee, 2004a), and hydromorphic processes (Taylor and Lagroix, 2015). Therefore, great caution is needed when interpreting the magnetic fabrics of paleosol units in paleowind investigations.

In terms of paleowind directions of loess layers, our AMS results for two parallel loess profiles show that in both sections, Dec-κ_{max} of the magnetic fabrics is preferentially distributed along the NW–SE direction (Figs. 7, 8). A previous AMS study of the loess deposits of the nearby BCY section (Huang and Sun, 2005; Fig. 10) also revealed a significant NW–SE orientation of Dec-κ_{max}, and similar AMS results were reported for the last glacial loess units of the XN section, which is located in the westernmost Loess Plateau (Ge et al., 2014; Fig. 10). The NW–SE orientation of Dec-κ_{max} of the magnetic fabric of the loess deposits is nearly parallel to the modern prevailing winter and summer monsoon wind directions (Fig. 1a). Modern meteorological

https://doi.org/10.1017/qua.2021.5 Published online by Cambridge University Press

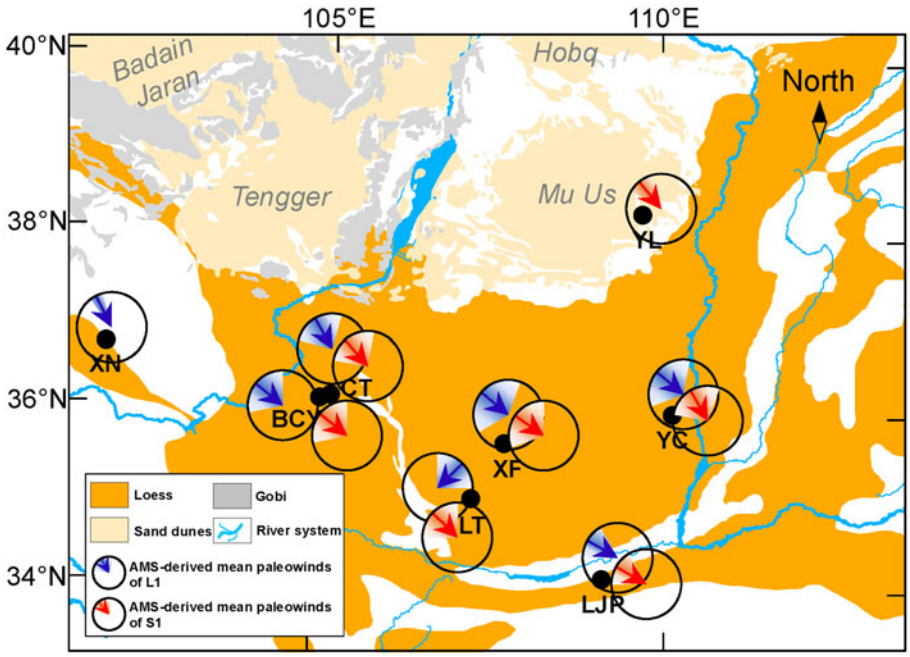

Figure 10. Paleowind directions derived from magnetic fabrics of loess sections from the Chinese Loess Plateau. Blue (AMS-derived mean paleowinds for L1-the last glacial loess) and red (AMS-derived mean paleowinds for S1-the last interglacial soil) arrows denote the mean direction of Dec-κ_{max} in the foliation plane and shaded areas denote the confidence angle. AMS results for various sections are: LJP (Liujiapo) section (Thistlewood and Sun, 1991); YL (Yulin) section (Sun et al., 1995); LT (Lingtai) section (Zhu et al., 2004); BCY (Baicaoyuan) section (Huang and Sun, 2005); XF (Xifeng) and YC (Yichuan) sections (Zhang et al., 2010); XN (Xining) section (Ge et al., 2014); CT (Caotan) section (this study). (For interpretation of the references to color in this figure legend, the reader is referred to the web version of this article.)

observations show that the southeasterly East Asian summer monsoon is mainly responsible for the moisture and heat delivery during summer, and the northwesterly East Asian winter monsoon is mainly responsible for the generation of modern dust storms and dust transportation during winter (Wang, 2006). Therefore, the present AMS results indicate that the dominant wind system responsible for the dust supplied to and deposited within the western Loess Plateau is the East Asian winter monsoon, with a prevailing NW direction.

The paleowind direction inferred from AMS studies in the western CLP is in striking contrast with the conclusions based on the U-Pb geochronology of single zircon grains from the Qaidam Basin (Pullen et al., 2011). Pullen et al. (2011) suggested that westerly winds dominated dust transport in the CLP during glacial periods, and that the loess deposits of the CLP were largely derived from the Qaidam Basin to the west. However, an increasing amount of geochemical evidence has led to the questioning of the role of the Qaidam Basin as a main source of dust supply to the CLP, and placed more emphasis on the contribution of aeolian dust from the northeastern Tibetan Plateau (TP), which is commonly defined as the region bounded by the Kunlun Mountains to the south and the Altun and the Qilian Mountains to the north (Fig. 1). Although the Qaidam Basin contains clastic materials from the southern Qilian and Kunlun Mountains (Wang et al., 2017; Nie et al., 2019), which are portions of the northeastern TP, it was not an actual dust source for the loess deposits of the CLP. Based on zircon grain ages, Che and Li (2013) argued that the contribution of aeolian dust from the Qaidam Basin to the main part of the Loess Plateau was negligible, and instead, a mixed contribution of materials from the northeastern TP and the Altay Mountains was suggested as the primary source of the loess deposits of the CLP. Based on a larger dataset of U-Pb ages and a new mixture-modeling statistic technique, Licht et al. (2016) suggested that the contribution of dust from the Qaidam Basin to loess deposits on the CLP was no more than 20%. Zhang et al. (2016) further revealed that the Tengger Desert and Mu Us sand dune field, combined with the northeastern TP, dominate the sediments of the CLP. A similar conclusion regarding dust contribution from the TP was also reached from recent analyses of Sr, Nd, and Hf isotopes (Bird et al., 2020). Thus, the contribution of eolian dust from the Qaidam Basin to the CLP was overestimated in Pullen et al. (2011).

The topography of the Qaidam Basin also militates against its role as an important dust source for the CLP. The Qaidam Basin is bounded on the south by the towering Kunlun Mountains, with numerous peaks in the western area exceeding 5000 m asl; and in the north and east by the Altun and Qilian mountain systems with many peaks exceeding 4500 m asl (Fig. 1a). The minimum difference in the relative elevation between the Qaidam Basin (average elevation 2400–3000 m) and the surrounding mountains is ~1500 m. As pointed out by Tsoar and Pye (1987) and Pye and Zhou (1989), the dust transport responsible for the formation of the loess deposits of the Loess Plateau occurs mainly in the lower 1500 m of the atmosphere. Thus, a large amount of the dust produced in the Qaidam Basin cannot be transported across the surrounding mountains by low-altitude winds and deposited on the Loess Plateau. The aeolian materials crossing these mountains are much finer-grained, and they are more likely to be part of the long-range dust component transported to the North Pacific by high-level (> 3000 m) westerly circulation (Gong et al., 2017; Nie et al., 2018; Sun et al., 2020). Therefore, based on atmospheric circulation patterns and geographical characteristics, the role of the Qaidam Basin as a major source of aeolian dust in the CLP can be excluded.

On glacial–interglacial timescales, the U-Pb geochronological evidence from the Qaidam Basin (Pullen et al., 2011) also suggested that the prevailing dust-bearing wind direction shifted to the northwest during interglacial periods, different from the direction during glacial and interstadial periods. Our AMS results from the paleosol units in both Section A and Section B show magnetic lineation directions intensively oriented along a NW–SE direction, consistent with the AMS results of the loess units (Figs. 7, 8). Similar AMS results were also reported for the nearby BCY section over the past 130 ka (Huang and Sun, 2005). These

https://doi.org/10.1017/qua.2021.5 Published online by Cambridge University Press

observations therefore suggest that the prevailing wind responsible for dust transport of the loess deposits in the western Loess Plateau is relatively stable on glacial–interglacial timescales.

For the eastern CLP, much sedimentary and AMS evidence also suggests that the northwesterly winds of the East Asian winter monsoon were the dominant transport mechanism for the loess deposits in north-central China. This inference has been confirmed by evidence of the fining of the aeolian grain size (Liu, 1985; Ding et al., 1999; Yang and Ding, 2008), a decrease in dust sedimentation rates (Lu and Sun, 2000), and the thinning of loess deposits (Wang et al., 2010) from northwest to southeast in the main part of the Loess Plateau. In addition, spatial variations in loess grain size from the past two glacial and interglacial cycles in the eastern Loess Plateau presented in Yang and Ding (2008) showed a near NW–SE gradient for both glacials and interglacials, also indicating a stable dust-transport pathway for the loess deposits in the CLP. Earlier AMS studies of the loess deposits of the LJP, YL, XF, and YC sections (see Fig. 10 for abbreviations and locations) also revealed a preferred orientation of Dec-κ_{max} along the NW–SE direction (Thistlewood and Sun, 1991; Sun et al., 1995; Zhang et al., 2010), which confirms the dominant role of the winter monsoon in transporting aeolian dust to the CLP. Recent AMS studies of the Neogene red clay sequences spanning from 7.0–2.6 Ma in the Lingtai section, and 11.0–2.6 Ma in the Shilou section, revealed that the Dec-κ_{max} of the magnetic fabrics are grouped in the NW quadrant (Gong et al., 2015), which likely indicates that the northwesterly winter monsoon played the dominant role in the transport of the dust even for pre-Quaternary aeolian deposits despite glacial and interglacial variations.

In summary, both the AMS results and independent sedimentary evidence indicate that for the entire CLP, the prevailing winds responsible for dust transport are the northwesterly winds of the East Asian winter monsoon during both glacial and interglacial intervals. Theoretically, the main sources of aeolian deposits are usually located in the upwind direction of the dust sink regions (e.g., the Chinese Loess Plateau). Our AMS results therefore imply that large areas of deserts and Gobi deserts (Liu, 1985; Sun, 2002; Sun et al., 2020), as well as Yellow River sediments (Nie et al., 2015; Licht et al., 2016) to the northwest of the CLP, may have been providing dust for loess deposits in the Loess Plateau at least for the last glacial and interglacial cycle. However, our results cannot distinguish the contribution of these specific, individual dust source areas that all lie in the upwind direction from the CLP along the prevailing East Asian winter monsoon winds.

CONCLUSION

We have studied the AMS of two parallel loess profiles spanning the past 130 ka in Caotan county, Gansu Province, in the western Chinese Loess Plateau. Our results show that the magnetic lineations of the loess units are significantly clustered along the NW to SE direction, consistent with the direction of the winds of the modern East Asian winter monsoon. This suggests that the East Asian winter monsoon creates the prevailing winds responsible for dust transport to the western Chinese Loess Plateau. Similar paleowind directions were derived from AMS results from paleosol units in both two sections, which suggests that the dust-bearing wind directions in the western Loess Plateau are relatively stable during glacial and interglacial cycles. Combined with sedimentary and AMS evidence from the eastern CLP, we conclude that the East Asian winter monsoon dominates dust transport across the entire Chinese Loess Plateau during both glacial and interglacial periods. Our AMS results highlight the large areas of deserts and Gobi deserts located in the upwind direction as the dominant sources of the aeolian deposits of the Loess Plateau.

Acknowledgments. We are grateful to France Lagroix, Junsheng Nie, and the editor Nicholas Lancaster for their constructive comments and suggestions, which improved the manuscript significantly; to Aleeya Rahman and Jan Bloemendal for language improvement. Special thanks are due to Shuangchi Liu and Huafeng Qin for their kind assistance with the magnetic measurements.

Financial Support. This study was jointly supported by the Strategic Priority Research Program of Chinese Academy of Sciences (award XDB26000000), the National Natural Science Foundation of China (awards 41888101, 41625010, and 41690114), and the National Key Research and Development Program (award 2017YFE0112800).

REFERENCES

Antoine, P., Goval, E., Jamet, G., Coutard, S., Moine, O., Hérisson, D., Auguste, P., *et al.*, 2014. The Upper Pleistocene loess sequences of Havrincourt (Pas-de-Calais, France): stratigraphy, paleoenvironments, geochronology and human occupations. *Quaternaire* **25**, 321–368. [in French with English abstract]

Arimoto, R., 2001. Eolian dust and climate: relationships to sources, tropospheric chemistry, transport and deposition. *Earth-Science Reviews* **54**, 29–42.

Banerjee, S.K., Hunt, C.P., Liu, X.M., 1993. Separation of local signals from the regional paleomonsoon record of the Chinese Loess Plateau: a rock-magnetic approach. *Geophysical Research Letters* **20**, 843–846.

Bird, A., Millar, I., Rodenburg, T., Stevens, T., Rittner, M., Vermeesch, P., Lu, H., 2020. A constant Chinese Loess Plateau dust source since the late Miocene. *Quaternary Science Reviews* **227**, 106042. https://doi.org/10.1016/j.quascirev.2019.106042.

Boyd, P.W., Watson, A.J., Law, C.S., Abraham, E.R., Trull, T., Murdoch, R., Bakker, D.C.E., *et al.*, 2000. A mesoscale phytoplankton bloom in the polar Southern Ocean stimulated by iron fertilization. *Nature* **407**, 695–702.

Bradák, B., Újvári, G., Seto, Y., Hyodo, M., Végh, T., 2018. A conceptual magnetic fabric development model for the Paks loess in Hungary. *Aeolian Research* **30**, 20–31.

Bullard, J.E., Baddock, M., Bradwell, T., Crusius, J., Darlington, E., Gaiero, D., Gassó, *et al.*, 2016. High-latitude dust in the Earth system. *Reviews of Geophysics* **54**, 447–485.

Che, X., Li, G., 2013. Binary sources of loess on the Chinese Loess Plateau revealed by U–Pb ages of zircon. *Quaternary Research* **80**, 545–551.

Constable, C., Tauxe, L., 1990. The bootstrap for magnetic susceptibility tensors. *Journal of Geophysical Research: Solid Earth* **95**, 8383–8395.

Deng, C., Vidic, N.J., Verosub, K.L., Singer, M.J., Liu, Q., Shaw, J., Zhu, R., 2005. Mineral magnetic variation of the Jiaodao Chinese loess/paleosol sequence and its bearing on long-term climatic variability. *Journal of Geophysical Research: Solid Earth* **110**. https://doi.org/10.1029/2004JB003451.

Deng, C., Zhu, R., Verosub, K.L., Singer, M.J., Yuan, B., 2000. Paleoclimatic significance of the temperature-dependent susceptibility of Holocene loess along a NW–SE transect in the Chinese loess plateau. *Geophysical Research Letters* **27**, 3715–3718.

Ding, Z.L., Derbyshire, E., Yang, S.L., Yu, Z.W., Xiong, S.F., Liu, T.S., 2002. Stacked 2.6-Ma grain size record from the Chinese loess based on five sections and correlation with the deep-sea $\delta^{18}O$ record. *Paleoceanography and Paleoclimatology* **17**, 5-1–5-21.

Ding, Z., Sun, J., Rutter, N.W., Rokosh, D., Liu, T., 1999. Changes in sand content of loess deposits along a North–South transect of the Chinese Loess Plateau and the implications for desert variations. *Quaternary Research* **52**, 56–62.

Ellwood, B.B., 1984. Bioturbation: minimal effects on the magnetic fabric of some natural and experimental sediments. *Earth and Planetary Science Letters* **67**, 367–376.

Gao, X., Hao, Q., Oldfield, F., Bloemendal, J., Deng, C., Wang, L., Song, Y., *et al.*, 2019. New high-temperature dependence of magnetic susceptibility-based climofunction for quantifying paleoprecipitation from Chinese loess. *Geochemistry, Geophysics, Geosystems* **20**, 4273–4291.

Ge, J., Guo, Z., Zhao, D., Zhang, Y., Wang, T., Yi, L., Deng, C., 2014. Spatial variations in paleowind direction during the last glacial period in north China reconstructed from variations in the anisotropy of magnetic susceptibility of loess deposits. *Tectonophysics* **629**, 353–361.

Gong, H., Xie, W., Wang, J., Zhang, R., Zhang, Y., Yang, L., 2017. Zircon U-Pb ages of quaternary loess-paleosol sequences from the Luochuan section: implication for sediment provenance. *Acta Geologica Sinica* **91**, 357–358. [English edition]

Gong, H., Zhang, R., Yue, L., Zhang, Y., Li, J., 2015. Magnetic fabric from Red clay sediments in the Chinese Loess Plateau. *Scientific Reports* **5**, 9706. https://doi.org/10.1038/srep09706.

Goudie, A.S., Middleton, N.J., 2006. *Desert Dust in the Global System*. Springer-Verlag, Berlin. 288 pp.

Graham, J.W., 1954. Magnetic anisotropy, an unexploited petrofabric element. *Geological Society of America Bulletin* **65**, 1257–1258.

Guo, J., Lou, M., Miao, Y., Wang, Y., Zeng, Z., Liu, H., He, J., *et al.*, 2017. Trans-Pacific transport of dust aerosols from East Asia: insights gained from multiple observations and modeling. *Environmental Pollution* **230**, 1030–1039.

Guo, Z.T., Ruddiman, W.F., Hao, Q.Z., Wu, H.B., Qiao, Y.S., Zhu, R.X., Peng, S.Z., Wei, J.J., Yuan, B.Y., Liu, T.S., 2002. Onset of Asian desertification by 22 Myr ago inferred from loess deposits in China. *Nature* **416**, 159–163.

Guo, Z.T., Sun, B., Zhang, Z.S., Peng, S.Z., Xiao, G.Q., Ge, J.Y., Hao, Q.Z., *et al.*, 2008. A major reorganization of Asian climate by the early Miocene. *Climate of the Past* **4**, 153–174.

Hadley, G., 1735. VI. Concerning the cause of the general trade-winds. *Philosophical Transactions of the Royal Society of London* **39**, 58–62.

Hao, Q., Guo, Z., 2007. Magnetostratigraphy of an early-middle Miocene loess-soil sequence in the western Loess Plateau of China. *Geophysical Research Letters* **34**. https://doi.org/10.1029/2007GL031162.

Hao, Q., Wang, L., Oldfield, F., Peng, S., Qin, L., Song, Y., Xu, B., Qiao, Y., Bloemendal, J., Guo, Z., 2012. Delayed build-up of Arctic ice sheets during 400,000-year minima in insolation variability. *Nature* **490**, 393–396.

Harrison, R.J., Feinberg, J.M., 2008. FORCinel: an improved algorithm for calculating first-order reversal curve distributions using locally weighted regression smoothing. *Geochemistry, Geophysics, Geosystems* **9**. https://doi.org/10.1029/2008GC001987.

Hrouda, F., 1982. Magnetic anisotropy of rocks and its application in geology and geophysics. *Geophysical Surveys* **5**, 37–82.

Huang, X.G., Sun, J.M., 2005. Study of the magnetic fabrics in Chinese loess-paleosols since the last interglacial: implication of the paleowind direction. *Quaternary Sciences* **25**, 516–522. [in Chinese with English abstract]

Hus, J.J., 2003. The magnetic fabric of some loess/palaeosol deposits. *Physics and Chemistry of the Earth, Parts A/B/C* **28**, 689–699.

Ising, G., 1943. On the magnetic properties of varved clay: line of investigation: Measurements on a varve series from Viby in southern Sweden, *Volume* **1**. *Arkiv för Matematik, Astronomi och Fysik* 29A, 37 p.

Jelinek, V., 1981. Characterization of the magnetic fabric of rocks. *Tectonophysics* **79**, T63–T67.

Kapp, P., Pelletier, J.D., Rohrmann, A., Heermance, R., Russell, J., Ding, L., 2011. Wind erosion in the Qaidam basin, central Asia: implications for tectonics, paleoclimate, and the source of the Loess Plateau. *GSA Today* **21**, 4–10.

Kinne, S., Pueschel, R., 2001. Aerosol radiative forcing for Asian continental outflow. *Atmospheric Environment* **35**, 5019–5028.

Lagroix, F., Banerjee, S.K., 2002. Paleowind directions from the magnetic fabric of loess profiles in central Alaska. *Earth and Planetary Science Letters* **195**, 99–112.

Lagroix, F., Banerjee, S.K., 2004a. Cryptic post-depositional reworking in aeolian sediments revealed by the anisotropy of magnetic susceptibility. *Earth and Planetary Science Letters* **224**, 453–459.

Lagroix, F., Banerjee, S.K., 2004b. The regional and temporal significance of primary aeolian magnetic fabrics preserved in Alaskan loess. *Earth and Planetary Science Letters* **225**, 379–395.

Licht, A., Pullen, A., Kapp, P., Abell, J., Giesler, N., 2016. Eolian cannibalism: reworked loess and fluvial sediment as the main sources of the Chinese Loess Plateau. *Geological Society of America Bulletin* **128**, 944–956.

Li, L., Chen, J., Chen, Y., Hedding, D.W., Li, T., Li, L., Liu, X., *et al.*, 2018. Uranium isotopic constraints on the provenance of dust on the Chinese Loess Plateau. *Geology* **46**, 747–750.

Lisiecki, L.E., Raymo, M.E., 2005. A Pliocene–Pleistocene stack of 57 globally distributed benthic $\delta^{18}O$ records. *Paleoceanography* **20**. https://doi.org/10.1029/2004PA001071.

Liu, Q., Deng, C., Yu, Y., Torrent, J., Jackson, M.J., Banerjee, S.K., Zhu, R., 2005. Temperature dependence of magnetic susceptibility in an argon environment: implications for pedogenesis of Chinese loess/palaeosols. *Geophysical Journal International* **161**, 102–112.

Liu, T., 1985. *Loess and the Environment*. China Ocean Press, Beijing. [in Chinese]

Liu, T.S., 1966. *Composition and Texture of Loess*. Science Press, Beijing. [in Chinese]

Liu, W., Sun, J., 2012. High-resolution anisotropy of magnetic susceptibility record in the central Chinese Loess Plateau and its paleoenvironment implications. *Science China Earth Sciences* **55**, 488–494.

Lowrie, W., 1989. Magnetic analysis of rock fabric. In: James, D.E. (Ed.), *Encyclopedia of Earth Sciences Series: Encyclopedia of Solid Earth Geophysics*, Springer, Boston. pp. 698–706.

Lu, H., Sun, D., 2000. Pathways of dust input to the Chinese Loess Plateau during the last glacial and interglacial periods. *Catena* **40**, 251–261.

Lu, H., Wang, X., Li, L., 2010. Aeolian sediment evidence that global cooling has driven late Cenozoic stepwise aridification in central Asia. *Geological Society of London Special Publications* **342**, 29–44.

Maher, B.A., Thompson, R., 1991. Mineral magnetic record of the Chinese loess and paleosols. *Geology* **19**, 3–6.

Manabe, S., 1969. Climate and the ocean circulation I: the atmospheric circulation and the hydrology of the Earth's surface. *Monthly Weather Review* **97**, 739 –774.

Martin, J.H., Coale, K.H., Johnson, K.S., Fitzwater, S.E., Gordon, R.M., Tanner, S.J., Hunter, C.N., *et al.*, 1994. Testing the iron hypothesis in ecosystems of the equatorial Pacific Ocean. *Nature* **371**, 123–129.

Matasova, G., Petrovský, E., Jordanova, N., Zykina, V., Kapička, A., 2001. Magnetic study of Late Pleistocene loess/palaeosol sections from Siberia: palaeoenvironmental implications. *Geophysical Journal International* **147**, 367–380.

Mathé, P.E., Rochette, P., Colin, F., 1997. The origin of magnetic susceptibility and its anisotropy in some weathered profiles. *Physics and Chemistry of the Earth* **22**, 183–187.

Muxworthy, A.R., Dunlop, D.J., 2002. First-order reversal curve (FORC) diagrams for pseudo-single-domain magnetites at high temperature. *Earth and Planetary Science Letters* **203**, 369–382.

Nawrocki, J., Gozhik, P., Łanczont, M., Pańczyk, M., Komar, M., Bogucki, A., Williams, I., Czupyt, Z., 2018. Palaeowind directions and sources of detrital material archived in the Roxolany loess section (southern Ukraine). *Palaeogeography, Palaeoclimatology, Palaeoecology* **496**, 121–135.

Nawrocki, J., Polechońska, O., Boguckij, A., Łanczont, M., 2006. Palaeowind directions recorded in the youngest loess in Poland and western Ukraine as derived from anisotropy of magnetic susceptibility measurements. *Boreas* **35**, 266–271.

Nie, J., Pullen, A., Garzione, C.N., Peng, W., Wang, Z., 2018. Pre-Quaternary decoupling between Asian aridification and high dust accumulation rates. *Science Advances* **4**. https://doi.org/10.1126/sciadv.aao6977.

Nie, J., Ren, X., Saylor, J.E., Su, Q., Horton, B.K., Bush, M.A., Chen, W., Pfaff, K., 2019 (2020). Magnetic polarity stratigraphy, provenance, and paleoclimate analysis of Cenozoic strata in the Qaidam Basin, NE Tibetan Plateau. *Geological Society of America Bulletin* **132**, 310–320.

Nie, J., Stevens, T., Rittner, M., Stockli, D., Garzanti, E., Limonta, M., Bird, A., *et al.*, 2015. Loess plateau storage of Northeastern Tibetan Plateau-derived Yellow River sediment. *Nature Communications* **6**, 8511. https://doi.org/10.1038/ncomms9511.

Owens, W.H., Bamford, D., 1976. A discussion on natural strain and geological structure—magnetic, seismic, and other anisotropic properties of rock fabrics. *Philosophical Transactions of the Royal Society of London Series A: Mathematical and Physical Sciences* **283**, 55–68.

Özdemir, Ö., Dunlop, D.J., Moskowitz, B.M., 1993. The effect of oxidation on the Verwey transition in magnetite. *Geophysical Research Letters* **20**, 1671–1674.

https://doi.org/10.1017/qua.2021.5 Published online by Cambridge University Press

Peng, S., Ge, J., Li, C., Liu, Z., Qi, L., Tan, Y., Cheng, Y., Deng, C., Qiao, Y., 2015. Pronounced changes in atmospheric circulation and dust source area during the mid-Pleistocene as indicated by the Caotan loess-soil sequence in North China. *Quaternary International* **372**, 97–107.

Pike, C.R., Roberts, A.P., Dekkers, M.J., Verosub, K.L., 2001. An investigation of multi-domain hysteresis mechanisms using FORC diagrams. *Physics of the Earth and Planetary Interiors* **126**, 11–25.

Pullen, A., Kapp, P., McCallister, A.T., Chang, H., Gehrels, G.E., Garzione, C.N., Heermance, R.V., Ding, L., 2011. Qaidam Basin and northern Tibetan Plateau as dust sources for the Chinese Loess Plateau and paleoclimatic implications. *Geology* **39**, 1031–1034.

Pye, K., Tsoar, H., 1987. The mechanics and geological implications of dust transport and deposition in deserts with particular reference to loess formation and dune sand diagenesis in the northern Negev, Israel. *Geological Society of London Special Publications* **35**, 139–156.

Pye, K., Zhou, L.P., 1989. Late Pleistocene and Holocene aeolian dust deposition in north China and the northwest Pacific Ocean. *Palaeogeography, Palaeoclimatology, Palaeoecology* **73**, 11–23.

Ridgwell, A.J., 2002. Dust in the Earth system: the biogeochemical linking of land, air and sea. *Philosophical Transactions of the Royal Society of London Series A: Mathematical, Physical and Engineering Sciences* **360**, 2905–2924.

Roberts, A.P., Heslop, D., Zhao, X., Pike, C.R., 2014. Understanding fine magnetic particle systems through use of first-order reversal curve diagrams. *Reviews of Geophysics* **52**, 557–602.

Roberts, A.P., Pike, C.R., Verosub, K.L., 2000. First-order reversal curve diagrams: a new tool for characterizing the magnetic properties of natural samples. *Journal of Geophysical Research: Solid Earth* **105**, 28461–28475.

Rochette, P., Fillion, G., Mattéi, J.L., Dekkers, M.J., 1990. Magnetic transition at 30–34 Kelvin in pyrrhotite: insight into a widespread occurrence of this mineral in rocks. *Earth and Planetary Science Letters* **98**, 319–328.

Rochette, P., Jackson, M., Aubourg, C., 1992. Rock magnetism and the interpretation of anisotropy of magnetic susceptibility. *Reviews of Geophysics* **30**, 209–226.

Rohrmann, A., Heermance, R., Kapp, P., Cai, F., 2013. Wind as the primary driver of erosion in the Qaidam Basin, China. *Earth and Planetary Science Letters* **374**, 1–10.

Smirnov, A.V., 2006. Low-temperature magnetic properties of magnetite using first-order reversal curve analysis: implications for the pseudo-single-domain state. *Geochemistry, Geophysics, Geosystems* **7**. https://doi.org/10.1029/2006GC001397.

Sokolik, I.N., Winker, D.M., Bergametti, G., Gillette, D.A., Carmichael, G., Kaufman, Y.J., Gomes, L., Schuetz, L., Penner, J.E., 2001. Introduction to special section: Outstanding problems in quantifying the radiative impacts of mineral dust. *Journal of Geophysical Research*: *Atmospheres* **106**, 18015–18027.

Sun, J., 2002. Provenance of loess material and formation of loess deposits on the Chinese Loess Plateau. *Earth and Planetary Science Letters* **203**, 845–859.

Sun, J., Huang, X., 2006. Half-precessional cycles recorded in Chinese loess: response to low-latitude insolation forcing during the Last Interglaciation. *Quaternary Science Reviews* **25**, 1065–1072.

Sun, J.M., Ding, Z.L., Liu, T.S., 1995. Primary application of magnetic susceptibility measurement of loess and paleosols for reconstruction of winter monsoon direction. *Chinese Science Bulletin* **40**, 1976–1978. [in Chinese]

Sun, Y., Clemens, S.C., Morrill, C., Lin, X., Wang, X., An, Z., 2012. Influence of Atlantic meridional overturning circulation on the East Asian winter monsoon. *Nature Geoscience* **5**, 46–49.

Sun, Y., Yan, Y., Nie, J., Li, G., Shi, Z., Qiang, X., Chang, H., An, Z., 2020. Source-to-sink fluctuations of Asian aeolian deposits since the late Oligocene. *Earth-Science Reviews* **200**. https://doi.org/10.1016/j.earscirev.2019.102963.

Tarling, D., Hrouda, F. (Eds.), 1993. *Magnetic Anisotropy of Rocks*. Chapman and Hall, London. 218 pp.

Taylor, S.N., Lagroix, F., 2015. Magnetic anisotropy reveals the depositional and postdepositional history of a loess-paleosol sequence at Nussloch (Germany). *Journal of Geophysical Research*: *Solid Earth* **120**, 2859–2876.

Thistlewood, L., Sun, J., 1991. A palaeomagnetic and mineral magnetic study of the loess sequence at Liujiapo, Xian, China. *Journal of Quaternary Science* **6**, 13–26.

Tsoar, H., Pye, K., 1987. Dust transport and the question of desert loess formation. *Sedimentology* **34**, 139–153.

Verosub, K.L., Fine, P., Singer, M.J., TenPas, J., 1993. Pedogenesis and paleoclimate: Interpretation of the magnetic susceptibility record of Chinese loess-paleosol sequences. *Geology* **21**, 1011–1014.

Wang, B., 2006. *The Asian Monsoon*. Springer Verlag, Berlin.

Wang, T., Wu, J., Kou, X., Oliver, C., Mou, P., Ge, J., 2010. Ecologically asynchronous agricultural practice erodes sustainability of the Loess Plateau of China. *Ecological Applications* **20**, 1126–1135.

Wang, W., Zheng, W., Zhang, P., Li, Q., Kirby, E., Yuan, D., Zheng, D., *et al.*, 2017. Expansion of the Tibetan Plateau during the Neogene. *Nature Communications* **8**, 15887. https://doi.org/10.1038/ncomms15887.

Wang, Y., Pan, B., Gao, H., Guan, Q., Chen, Y., Wang, J., 2007. Magnetic fabric-based reconstruction of the paleowind direction from a loess sequence in the northeastern flank of the Qilian mountains. *Chinese Journal of Geophysics* **50**, 1005–1010.

Wu, H.B., Chen, F.H., Wang, J.M., Cao, J.X., Zhang, Y.T., 1998. A study on the relationship between magnetic anisotropy of modern eolian sediments and wind direction. *Chinese Journal of Geophysics* **41**, 811–817. [in Chinese with English abstract]

Wu, L., Prush, V., Lin, X., Xiao, A., Zhang, L., Chen, N., Yang, R., Chen, H., 2019. Quantifying wind erosion during the late Quaternary in the Qaidam Basin, Central Asia. *Geophysical Research Letters* **46**, 6378–6387.

Yang, S., Ding, Z., 2008. Advance–retreat history of the East-Asian summer monsoon rainfall belt over northern China during the last two glacial–interglacial cycles. *Earth and Planetary Science Letters* **274**, 499–510.

Zeeden, C., Hambach, U., Händel, M., 2015. Loess magnetic fabric of the Krems-Wachtberg archaeological site. *Quaternary International* **372**, 188–194.

Zhang, H., Lu, H., Xu, X., Liu, X., Yang, T., Stevens, T., Bird, A., Xu, Z., Zhang, T., Lei, F., Feng, H., 2016. Quantitative estimation of the contribution of dust sources to Chinese loess using detrital zircon U-Pb age patterns. *Journal of Geophysical Research*: *Earth Surface* **121**, 2085–2099.

Zhang, R., Kravchinsky, V.A., Zhu, R., Yue, L., 2010. Paleomonsoon route reconstruction along a W–E transect in the Chinese Loess Plateau using the anisotropy of magnetic susceptibility: Summer monsoon model. *Earth and Planetary Science Letters* **299**, 436–446.

Zhang, X.Y., Gong, S.L., Zhao, T.L., Arimoto, R., Wang, Y.Q., Zhou, Z.J., 2003. Sources of Asian dust and role of climate change versus desertification in Asian dust emission. *Geophysical Research Letters* **30**. https://doi.org/10.1029/2003GL018206.

Zhao, H., Sun, Y., Qiang, X., 2017. Iron oxide characteristics of mid-Miocene Red Clay deposits on the western Chinese Loess Plateau and their paleoclimatic implications. *Palaeogeography, Palaeoclimatology, Palaeoecology* **468**, 162–172.

Zhou, L.P., Oldfield, F., Wintle, A.G., Robinson, S.G., Wang, J.T., 1990. Partly pedogenic origin of magnetic variations in Chinese loess. *Nature* **346**, 737–739.

Zhu, R., Liu, Q., Jackson, M.J., 2004. Paleoenvironmental significance of the magnetic fabrics in Chinese loess-paleosols since the last interglacial (<130 ka). *Earth and Planetary Science Letters* **221**, 55–69.

https://doi.org/10.1017/qua.2021.5 Published online by Cambridge University Press